Ceramics International 48 (2022) 12897–12905

Contents lists available at ScienceDirect

Ceramics International

journal homepage: www.elsevier.com/locate/ceramint

Developing Nickel/Graphene Nano Sheets as an alternative primary battery anode

Rikson Siburian [a,b,*], Suriati Paiman [c], Fajar Hutagalung [a], Ab Malik Marwan Ali [d], Lisnawaty Simatupang [e], Ronn Goei [f], Mohamad Mahmood Rusop [g,h]

[a] Postgraduate Program, Chemistry Department, Faculty of Mathematics and Natural Sciences, Universitas Sumatera Utara, Medan, Indonesia
[b] Carbon Research Center-Universitas Sumatera Utara, Medan, Indonesia
[c] Physics Department, Faculty of Science, Universiti Putra Malaysia, 43400, Serdang, Seri Kembangan, Selangor, Malaysia
[d] Faculty of Applied Sciences, Universiti Teknologi MARA, 40450, Shah Alam, Selangor, Malaysia
[e] Department of Chemistry- Faculty of Mathematics and Natural Sciences, Universitas Negeri Medan, Medan, Indonesia
[f] School of Materials Science and Engineering, Nanyang Technological University, 50 Nanyang Avenue, 639798, Singapore
[g] School of Electrical Engineering, College of Engineering, Universiti Teknologi MARA, 40450, Shah Alam, Selangor, Malaysia
[h] NANO-SciTech Lab (NST), Center for Functional Materials and Nanotechnology, Institute of Science (IOS), Universiti Teknologi MARA, 40450, Shah Alam, Selangor, Malaysia

ARTICLE INFO

Keywords:
Ni/Graphene Nano Sheet
Electrode battery
Anode battery
Alternatives electrode
p-d interaction

ABSTRACT

In this paper, we report the development of Nickel (Ni)/Graphene Nano Sheets (GNS) as a primary battery anode. The research focuses on the effect of Ni particle sizes on the performance of Ni/GNS anode. GNS and Ni/GNS (Ni wt% from 10 to 40%) are synthesized using the modified Hummers and impregnation method. We employed the use of commercial Zn-plate as an anode reference material. The materials are characterized with XRD, EDX, SEM, TEM and electrical conductivity meter. The XRD spectra of Ni-GNS have the broad and weak peaks at $2\theta = 26.77$ and 44.55° identified as C (002) and Ni (111), respectively. The XRD data is consistent with data obtained from EDX analysis which showed the presence of C and Ni at 0.277 and 7.472 keV respectively. The smallest Ni particle sizes of 23.4 nm was synthesized from Ni(20%)/GNS, Interestingly, the small particle size of Ni may improve the electrical conductivity of Ni/GNS. We found that Ni(20%)/GNS (62.2 μS/cm^2) has a higher electrical conductivity value than GNS (61.4 μS/cm^2) with commercial primary battery anodes Zn plate showing electrical conductivities of 35 μS/cm^2. We therefore proposed the potential of Ni/GNS to be developed as alternative materials for primary battery anode.

1. Introduction

Commercial batteries consist of several main components, namely cathode, anode, electrolyte, separator and current collector [1–3]. The anode acts as a source of electrons in the battery electrochemical system [4]. Some examples of anode materials that are widely used in commercial batteries are Zn, Li, graphite, and $Li_4Ti_5O_{12}$ [2,3,5]. The main problems associated with the use of anode materials in commercial battery systems today are: (i) short battery life due to inability of Zn and Li metals to control electron mobility rate [6–8], (ii) the use of lithiophilic LiC_6 as anode may cause internal short circuit and possible damage on the battery due to the dendrite growth on the anode surface when operating at a high current density [9–11], (iii) the natural availability of raw Zn and Li is limited [12], (iv) high production and commercialization costs [8], and (v) the low performance of the battery in terms of its energy density, electrical conductivity and capacity [13–15]. The use of graphene as an anode material improves the electrical properties and provides good chemical stability to the battery [16]. The use of Wrinkled Graphene Nanosheet as the anode of a Li-ion battery showed a specific energy of ~404 mAh g^{-1} at 2 A g^{-1} with a high Coulombic efficiency (~96%) at 300 mAh g^{-1} and a stable cycle life of up to 200 cycles [17]. The present works discuss the preparation of alternatives anode materials through metal deposition on graphene nano sheet. The interaction between metal particles and graphene through the metal adsorption process on the graphene surface can improve and modify the resulting electronic and magnetic properties of the graphene

* Corresponding author. Postgraduate Program, Chemistry Department, Faculty of Mathematics and Natural Sciences, Universitas Sumatera Utara, Medan, Indonesia.
E-mail address: rikson@usu.ac.id (R. Siburian).

https://doi.org/10.1016/j.ceramint.2022.01.162
Received 11 December 2021; Received in revised form 11 January 2022; Accepted 15 January 2022
Available online 29 January 2022

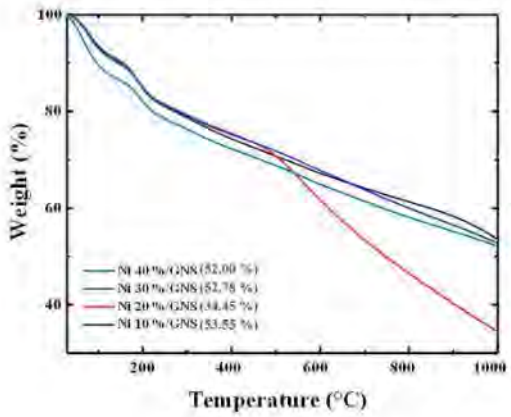

Fig. 1. TGA data of Ni/GNS.

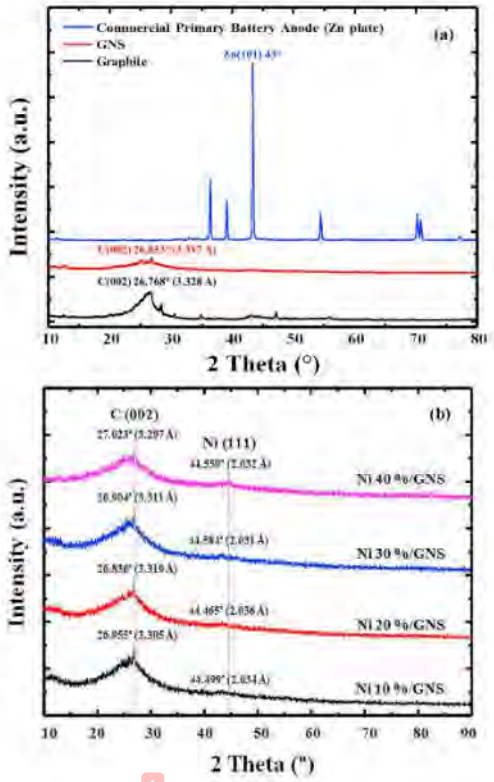

Fig. 2. Diffractogram of Commercial Primary Battery Anode (Zn plate), GNS, and Graphite (a), and Ni/GNS (b).

composite [18]. Graphene sheets can minimize the occurrence of metal particle agglomeration, and are able to control the size distribution and distribution of metal particles deposited on the surface of the sheet [19–21]. The application of Ni/graphene composite in the manufacture

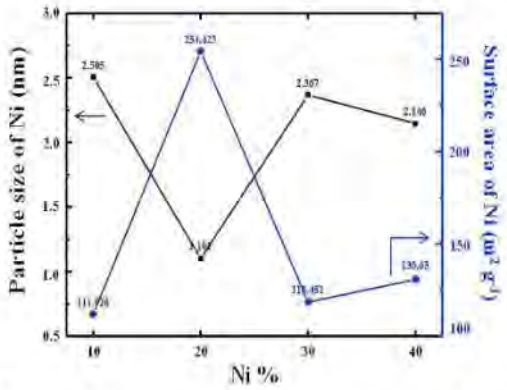

Fig. 3. Size and surface area of Ni particles deposited on the surface of GNS.

of battery electrodes would enhance the performance (electrical conductivity, energy density and capacity) of the primary battery [22]. This work also investigate the effect of the interaction of GNS with Ni (d-block metal) as well as the effect on the concentration of Ni on the final deposited metal particle size with the resulting performance (electrical conductivity) of the battery. To the best of the author knowledge, this is the first time of such interaction is being investigated.

2. Materials and methodology

Preparation of Ni/GNS composite: A total of 0.5 g of GNS powder and 0.2250 g of $NiCl_2{\cdot}6H_2O$ crystals were added to each of 20 mL of ethanol and stirred for an hour to produce a mixture of GNS and Ni precursor solution. Next, a mixture of GNS and Ni precursor solution were mixed and stirred for further 3 h. The Ni-GNS mixture was filtered through Whatmann No. 42 filter paper to separate the precipitate. The precipitate obtained was dried at 80 °C for 2 h, producing a solid Ni 10%/GNS. The same procedure was carried out to prepare Ni/GNS with 20–40% Ni content by using 0.5062; 0.8678; and 1.3499 g $NiCl_2{\cdot}6H_2O$, respectively [23,24] The resulting powder were characterized by using thermogravimetric analyser (TGA), X-rays diffractometer (XRD), scanning electron microscope with energy dispersive X-rays (SEM-EDX), transmission electron microscope (TEM) and electrical conductivity meter.

Weight percentage analysis of Ni metal in Ni/GNS was carried out using a TGA instrument type Netzsch TG 209F3 TGA in N_2 atmosphere with a temperature range of 30–1000 °C (10.0 (° C/min)). The crystallographic analysis of Ni/GNS material with XRD was carried out to determine the size of Ni particles deposited on the surface of GNS. Structural analysis of Ni/GNS composite were performed using a PAN-Alytical X-ray diffractometer instrument 2–90°, scan speed 5° min^{-1}, accelerating voltage 45 kV and a current of 40 mA. SEM-EDX was used to study the morphology and to determine particle sizes of Ni on GNS as well as elemental composition of Ni/GNS composite. Further, surface morphology analysis of GNS and Ni/GNS materials were carried out with a TEM instrument (JEOL JEM-2100F) with accelerating voltage of 200 kV. Finally, the effect of the size on Ni metals deposited on the surface of the GNS and their activities were determined by measuring the electrical conductivity of the electrode. Electrical conductivity analysis was carried out on each of Ni/GNS using a fuse tube (length = 2.3 cm; diameter = 0.3 cm) containing each sample (mass = 0.15 g) combined with a DC Power Supply instrument CODY 3005DT and a ZOTEK ZT98 digital multimeter.

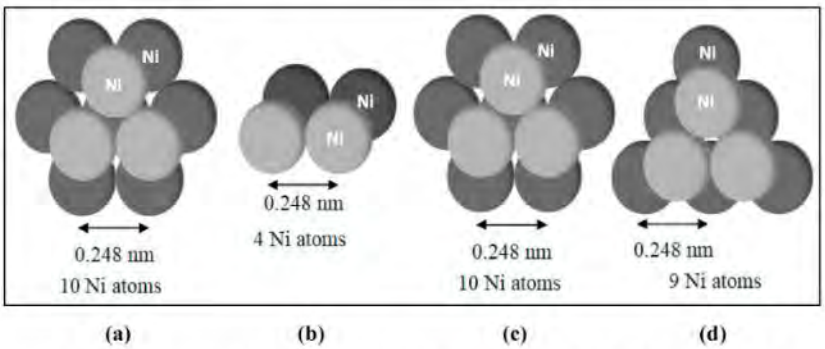

Fig. 4. Model of Ni particles deposited on the GNS surface: Ni 10%/GNS (a); Ni 20%/GNS (b); Ni 30%/GNS (c); Ni 40%/GNS (d).

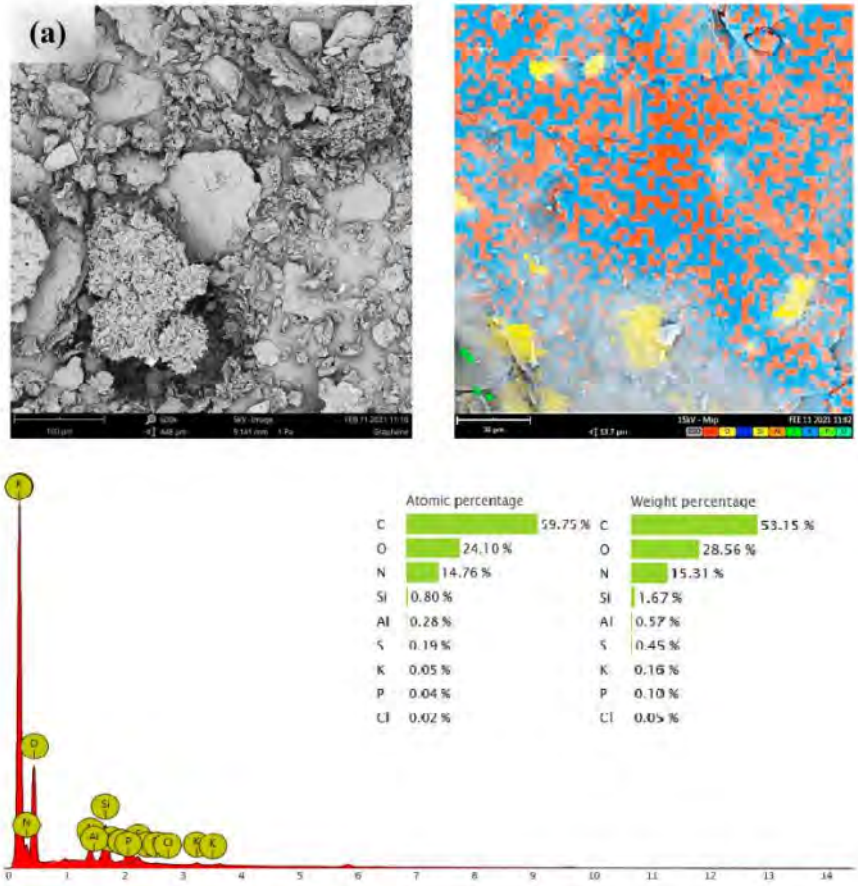

Fig. 5. SEM-EDX results and particle size of: GNS (a); Ni 10%/GNS (b); Ni 20%/GNS (c); Ni 30%/GNS (d); Ni 40%/GNS (e).

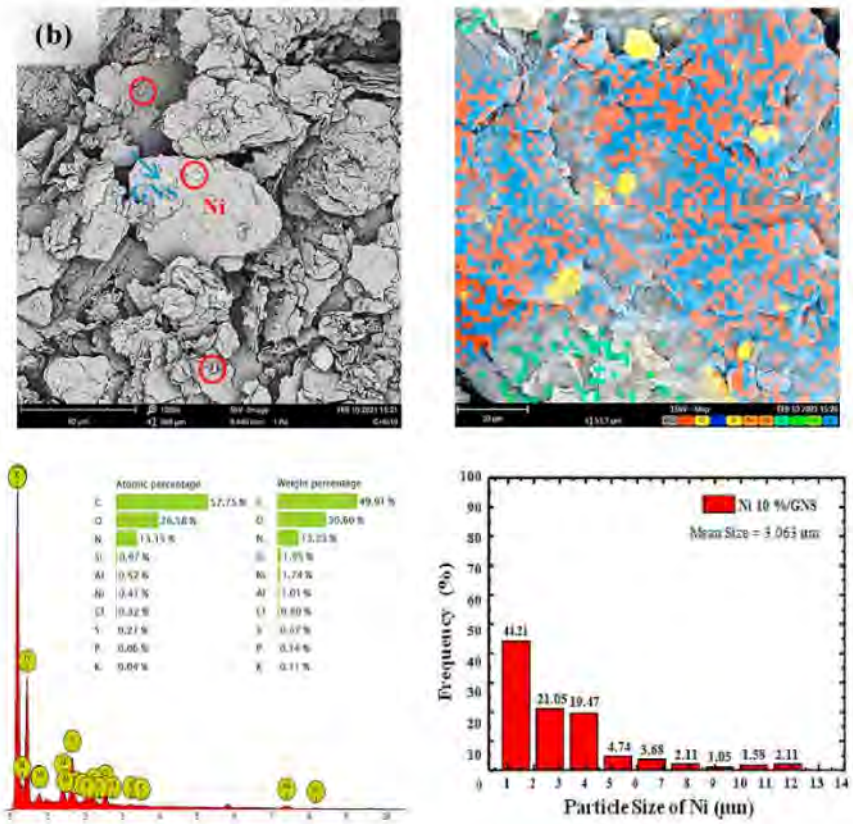

Fig. 5. (*continued*).

3. Results and discussion

TGA was used to evaluate the exact amounts of Ni deposited on the surface of GNSwith the result presented in Fig. 1. The thermogram pattern of Ni/GNS shows that Ni 20%/GNS has a different thermogram pattern with Ni 10, 30 and 40%/GNS. This is caused by the different sizes of the Ni particles deposited on the GNS surface. Ni 20%/GNS has a high weight loss of Ni starting at 500 °C compared to Ni 10, 30 and 40%/GNS. This is due to Ni 20%/GNS has the smallest particle size and number of Ni particles deposited on the GNS surface (as confirmed by XRD and SEM data).

The XRD diffractogram of GNS, commercial primary battery anode (Zn plate) and Ni/GNS are shown in Fig. 2. It shows the spectra of a commercial primary battery anode, graphite and GNS. XRD diffraction pattern of the graphite and GNS exhibit the peaks of C (002) at $2\theta = 26.768^{\circ}$ (3.328 Å) and 26.853° (3.317 nm) respectively which correspond to graphite (JCPDS 75–2078). On the other hand, the anode of commercial primary battery shows a peak at position $2\theta = 43^{\circ}$ which indicates that the anode of commercial primary battery is dominated by Zn (101) metal. The diffractogram pattern of Ni/GNS (Fig. 2(b)) shows the presence of weak and wide peaks at positions $2\theta = 26.836^{\circ}$ (3.319 Å), 26.904° (3.311 Å), 26.955° (3.305 Å) and 27.023° (3.297 Å) (peak typical of C (002) of GNS(JCPDS 75–2078). In addition, the diffraction peaks of Ni (111) where appear at positions $2\theta = 44.499^{\circ}$, 44.465°, 44.584°, and 44.550° prove the presence of Ni metal deposited on the GNS surface (JCPDS 87–0712) [25,26]. The diffractogram of Ni/GNS (Fig. 2(b)) also shows the intensity and diffraction peak shape of the Ni which changes with the increase in weight percentage of the Ni precursor used. This means that the Ni particles deposited on the GNS surface each have different sizes. Therefore, the particle size of the deposited Ni was calculated using the Scherrer equation [27].The size and surface area of the Ni particles deposited on the GNS surface based on calculations by the Scherrer method (Eq. (1) and (2)) are shown in Fig. 3.

Next, based on the results of the calculation of the number of clustered Ni particles (Fig. 3), the description of the model of Ni particles deposited on the GNS surface are presented in Fig. 4. Fig. 4 shows that the Ni particles deposited on the surface of the GNS form clusters. The darker color contrast that appears in each cluster arrangement of Ni particles deposited on the GNS surface indicates the location of the Ni particles which are farther from the reader's view. Ni 20%/GNS has a Ni particle size of 2.505 nm. The distance between Ni–Ni atoms in a cluster arrangement is 0.248 nm, so that the Ni 20%/GNS cluster is composed of 10 Ni atoms. There are two main factors that influence the formation of Ni clusters on the GNS surface, namely the entropy factor and the enthalpy factor. For the entropy factor, GNS with large surface area function as a supporting material and it is able to modify the electronic states of the deposited metal particles [28,29]. The second one (enthalpy factor), the overlapping of C–p_z orbital (graphene) with Ni–$3d_z^2$ (strong *p-d* hybridization)) which result in the charge transfer from Ni to graphene (n-doping graphene). Interfacial hybridization between Ni-graphene can open the graphene energy gap ($\Delta E_K = 0.32$ eV) [30,31]

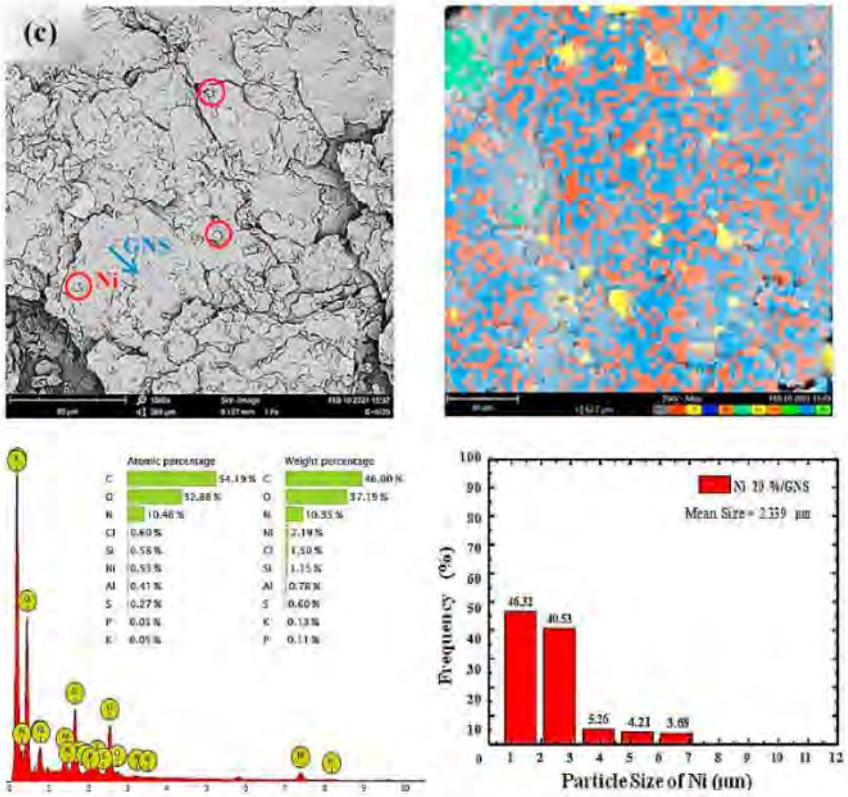

Fig. 5. (*continued*).

and is able to change the character of Ni metal and modify the particle size of Ni metal deposited on the graphene surface [18,32,33].

The surface morphology and components of Ni 10–40%/GNS based on the results of SEM-EDX analysis are shown in Fig. 5. The SEM image of Ni/GNS (Fig. 5(b–e)) shows that in each image there are small white spots (annotated by a red circles) which are clustered. Ni particles attached to thin sheets (GNS, annotated by blue arrows). The EDX mapping of Ni/GNS also shows the abundance of Ni/GNS constituent elements, where in each material there is the presence of carbon (GNS) and Ni elements. This indicates that the Ni metal particles have been uniformly deposited on the surface of the GNS. The EDX spectrum of Ni/GNS showed peaks at the energy values of 0.277 keV and 7.472 keV which correspond to C and Ni, respectively. The weight and atomic percentages of Ni deposited in the GNS increased in number with the increase in weight percentage of the Ni precursors. These results prove that each of the Ni metal has been deposited on the surface of the GNS. The EDX spectrum of Ni/GNS also showed the presence of other elements (Al and Si) which may come from the material residue left on the SEM-EDX sample holder. Fig. 5 also shows the size distribution and average size of Ni particles in Ni/GNS. The size of the deposited Ni particles is not linear with the concentration of Ni metal. Ni 20%/GNS has the smallest average Ni particle size of 2.339 μm and Ni 10%/GNS has the largest average Ni particle size of 3.063 μm. Ni/GNS composite exhibited a homogeneous deposited metal particle size distribution on the GNS surface. This proves that GNS is able to modify the character of Ni particles.

TEM analysis result of GNS (Fig. 6(a)) shows that the GNS structure consisted of thin non-uniform sheets with some wrinkles and folds at the edges caused by the chemical peeling treatment of the graphite structure. Based on the electron diffraction pattern of GNS, it can be observed that the internal point has a brighter light intensity than the other external points, proving that GNS is amorphous with fewer layers than graphite. Fig. 6(b–e) show the presence of black spots (indicated as Ni particles) attached to the GNS thin sheet. Electron diffraction results from Ni/GNS (Fig. 6(b–e)) show diffraction points and rings confirming the presence Ni (111) cluster on the surface of GNS. Based on the TEM images of Ni/GNS, the size of the Ni particles deposited on the GNS surface can be obtained. Ni 10%/GNS and Ni 30%/GNS have Ni particles deposited with sizes of 1.663 nm and 1.097 nm, while Ni 20%/GNS and Ni 40%/GNS have Ni particles deposited with sizes of 0.844 nm and 0.893, respectively, which means that the deposited Ni particles are Ni sub-nanocluster particles. These results prove that Ni/GNS was successfully synthesized and the surface of GNS is able to modify the size and character of the deposited Ni metal particles.

The results of the electrical conductivity measurement of commercial primary battery anode (Zn plate), GNS and Ni/GNS at a voltage of 1–30 V are shown in Fig. 7. The electrical conductivity of a commercial primary battery anode (Zn plate) shows a constant increasing value (Fig. 7).

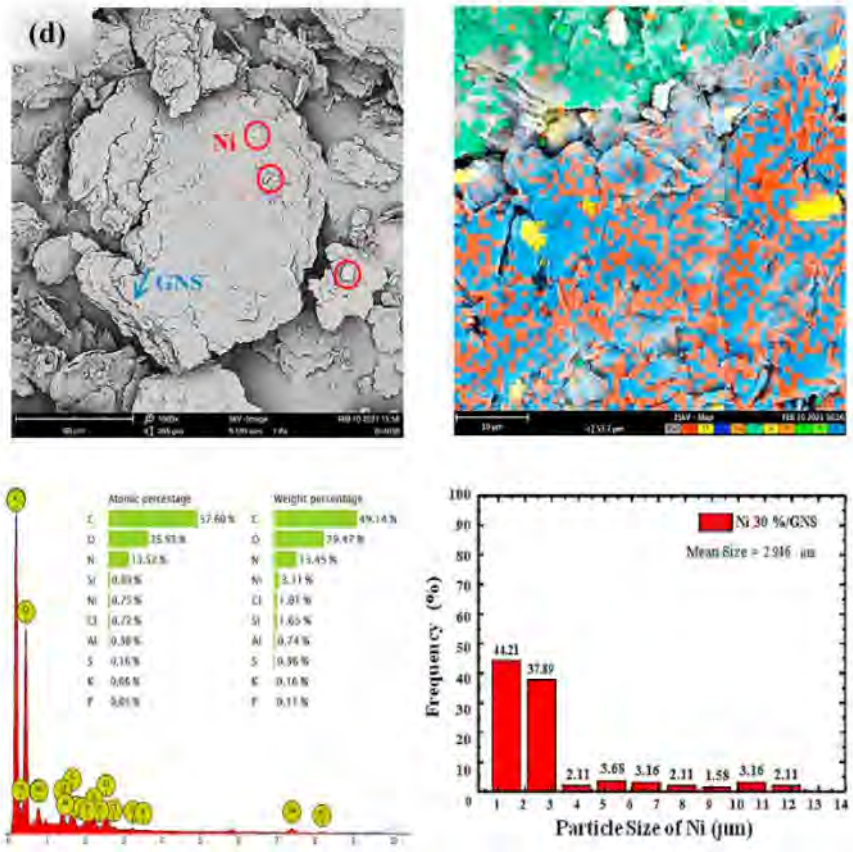

Fig. 5. (*continued*).

This proves that the anode of the primary battery is good enough to control the rate of electron mobility. GNS has a higher electrical conductivity value than commercial primary battery anodes. This is because GNS has delocalized electrons along the C = C bond which acts as an electric charge carrier. In addition, GNS also has a large surface area that would eventually increase the rate of electron mobility [34]. The value of electrical conductivity in the GNS increased significantly at a voltage of 1–9 V, then decreased at a voltage of 10–14 V, and increased again at a voltage of 14–30 V. This proves that the GNS is still difficult to control the mobility of electrons flowing through the external circuit. Ni/GNS has an increased electrical conductivity value and tends to be more stable than GNS. The metal-graphene alloy has a high surface to volume ratio so that it would improve the stability of the flow rate of electron mobility [35]. The electrical conductivity of Ni/GNS increases constantly at 1–6 V. Under these conditions, the electron flow rate increases gradually as the voltage increases. Electron mobility becomes more stable at 6–21 V. In this condition, the electron flow rate is laminar (laminar flow), where the kinetic energy of the electrons increases constantly, so the electrical conductivity increases slowly (more stable). At higher voltages (21–30 V), the kinetic energy used by electrons to move from the valence band to the conduction band increases excessively (turbulence flow) so that the electron flow rate becomes more active and faster that would reduce the resistivity and increase the electrical conductivity value of the electron significantly in each material. This proves that the greater the electric voltage applied to a material can increase the number and rate of electron mobility that flows.

Ni 20%/GNS has the highest electrical conductivity value (62.2 µS/cm^2) at the maximum voltage (30 V). This is because Ni 20%/GNS has the smallest average size of Ni metal particles deposited among other Ni/GNS (as confirmed by XRD and SEM data). The electrical conductivity values of Ni/GNS are each influenced by the size of the Ni metal particles deposited on the surface of the GNS. The smaller the size of metal particles deposited on the surface of the GNS would increase the surface contact area with the GNS resulting in an increase the activity of the GNS in conducting electric current (increased electrical conductivity). The use of metal clusters on graphene with smaller sizes can produce materials with more stable reactivity and electrical properties as well as higher electrical conductivity values [34]. Furthermore, to find out the comparison of the stability of commercial primary battery anodes (Zn plates), GNS, and Ni 20%/GNS in conducting electric current, electrical conductivity measurements were carried out for each material at a constant voltage (30 V) with a time variation of 5–60 min. Electrical conductivity measurements were carried out at 30 V corresponds to the maximum electrical conductivity value of each material was obtained.

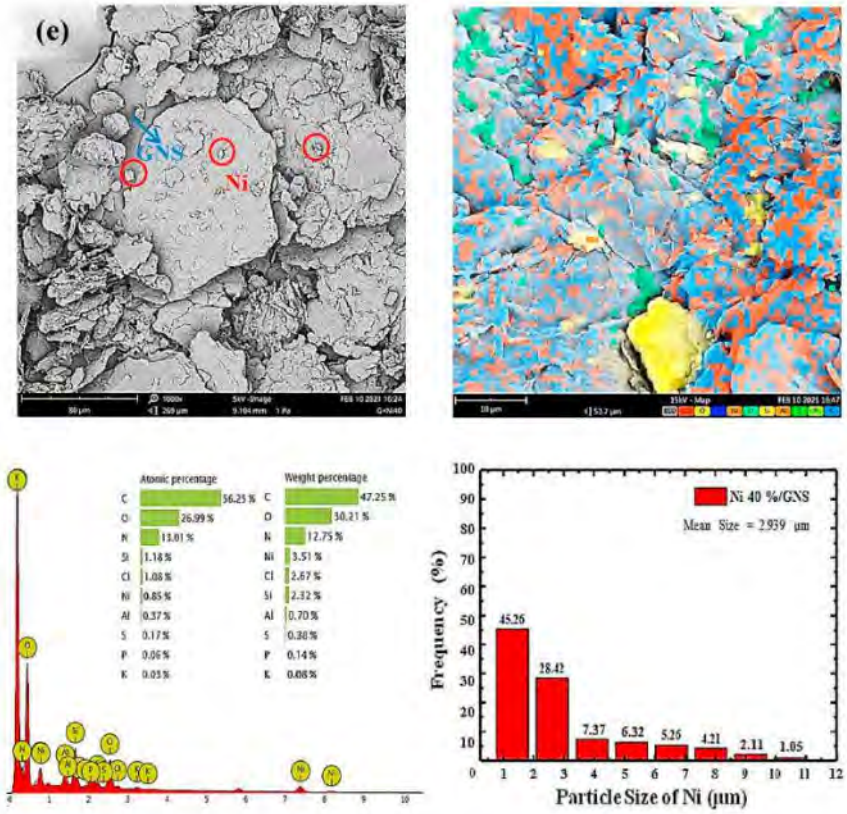

Fig. 5. (*continued*).

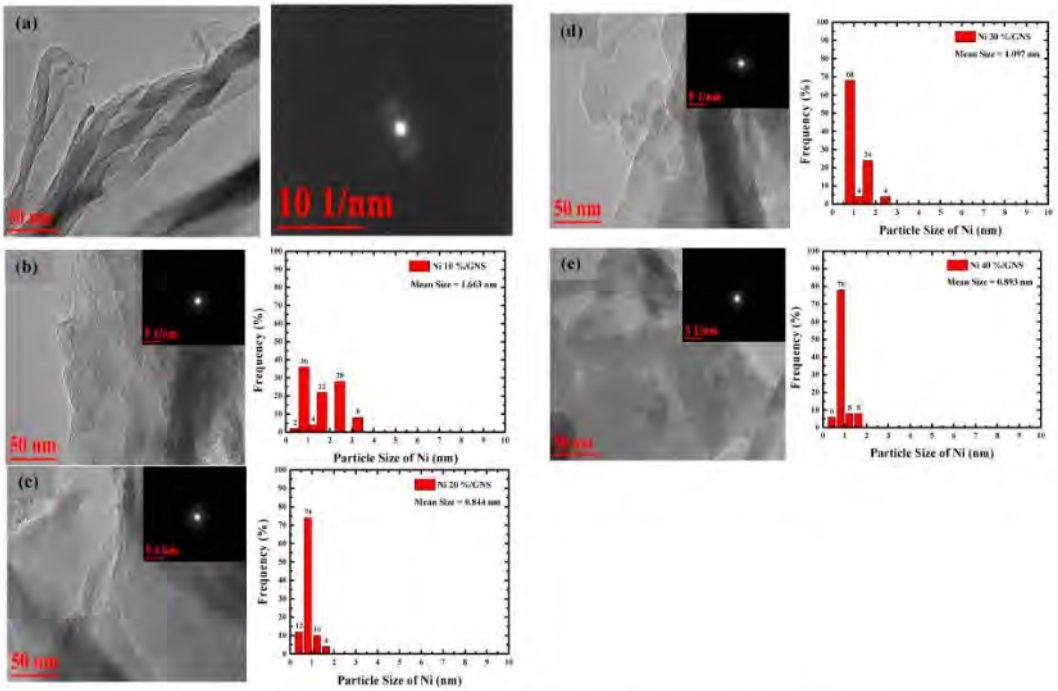

Fig. 6. TEM images of GNS (a); Ni 10%/GNS (b); Ni 20%/GNS (c); Ni 30%/GNS (d); and Ni 40%/GNS (e).

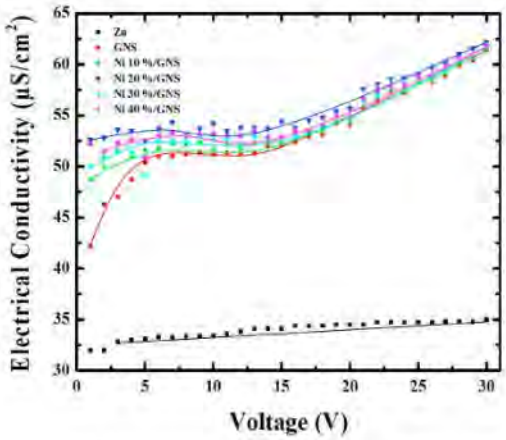

Fig. 7. Electrical Conductivity of Commercial Primary Battery Anode (Zn plate), GNS and Ni/GNS at a voltage of 1–30 V.

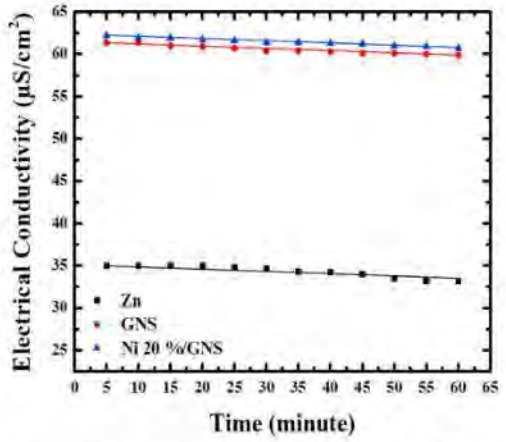

Fig. 8. Relationship of Electrical Conductivity (μS/cm^2) with Time (minutes) of commercial primary battery anode (Zn plate), GNS, and Ni 20%/GNS.

The electrical conductivity values of each material obtained at a voltage of 30 V (5–60 min) are presented in Fig. 7.

Fig. 8 shows that the Zn plate (commercial primary battery anode) has the largest reduction in electrical conductivity value (5.14%) compared to GNS (2.44%), and Ni 20%/GNS (2.41%) at 5–60 min and a constant voltage of 30 V. This is influenced by the nature of Zn metal which easily loses electrons at a given high voltage (30 V).

4. Conclusion

The interaction between GNS (supporting material) and Ni metal (*p-d*) can modify the character of Ni metal (covalent). The size of the Ni particles deposited on the GNS surface is not linear with the Ni precursor concentration. Ni 20%/GNS each has the smallest average size of Ni metal particles deposited in GNS, which is 2.339 μm, while Ni 10%/GNS has the largest average size of Ni metal particles deposited in GNS, which is 3.063 μm (SEM data).

Ni 20%/GNS (62.2 μS/cm^2) has a higher electrical conductivity value than GNS (61.4 μS/cm^2) and commercial primary battery anode (Zn plate, 35 μS/cm^2) so that it can be used as an alternative battery anode.

Declaration of competing interest

The authors declare that they have no known competing financial interests or personal relationships that could have appeared to influence the work reported in this paper.

Acknowledgments

The authors would like to thank Direktur Sumber Daya, Direktorat Jenderal Pendidikan Tinggi, Riset dan Teknologi and LPDP who funded this research under World Class Professor (WCP) Scheme Program No 2817/E4.1/KK.04.05/2021.

References

[1] R. Borah, F.R. Hughson, J. Johnston, T. Nann, On battery materials and methods, Mater. Today Adv. (2020), https://doi.org/10.1016/j.mtadv.2019.100046.
[2] N. Nitta, F. Wu, J.T. Lee, G. Yushin, Li-ion battery materials: present and future, Mater. Today (2015), https://doi.org/10.1016/j.mattod.2014.10.040.
[3] A.M. Haregewoin, A.S. Wotango, B.J. Hwang, Electrolyte additives for lithium ion battery electrodes: progress and perspectives, Energy Environ. Sci. (2016), https://doi.org/10.1039/C6EE00123H.
[4] M. Walter, M.V. Kovalenko, K.V. Kravchyk, Challenges and benefits of post-lithium-ion batteries, New J. Chem. (2020), https://doi.org/10.1039/C9NJ05mh2C.
[5] L. Zhang, J.D. Zhang, B.J. Xu, High-rate performance of polyethylene glycol-modified $Li_4Ti_5O_{12}$ anode materials, Results Phys. (2020), https://doi.org/10.1016/j.rinp.2020.103583.
[6] C. Hou, Q. Zhang, M. Zhu, Y. Li, H. Wang, One-step synthesis of magnetically-functionalized reduced graphite sheets and their use in hydrogels, Carbon (2011), https://doi.org/10.1016/j.carbon.2010.06.040.
[7] S. Dühnen, J. Betz, M. Kolek, R. Schmuch, M. Winter, T. Placke, Toward green battery cells: perspective on materials and technologies, Small Methods (2020), https://doi.org/10.1002/smtd.202000039.
[8] Q. Guo, W. Zeng, S.L. Liu, Y.Q. Li, J.Y. Xu, J.X. Wang, Y. Wang, Recent developments on anode materials for magnesium-ion batteries: a review, Rare Met. (2020), https://doi.org/10.1007/s12598-020-01493-3.
[9] S. Higashi, S.W. Lee, J.S. Lee, K. Takechi, Y. Cui, Avoiding short circuits from zinc metal dendrites in anode by backside-plating configuration, Nat. Commun. (2016), https://doi.org/10.1038/ncomms11801.
[10] A. Jana, D.R. Ely, R.E. García, Dendrite-separator interactions in lithium-based batteries, J. Power Sources (2015), https://doi.org/10.1016/j.jpowsour.2014.11.056.
[11] M.R. Al Hassan, A. Sen, T. Zaman, M.S. Mostari, Emergence of graphene as a promising anode material for rechargeable batteries: a review, Mater. Today Chem. (2019), https://doi.org/10.1016/j.mtchem.2018.11.006.
[12] J.F. Parker, C.N. Chervin, I.R. Pala, M. Machler, M.F. Burz, J.W. Long, D.R. Rolison, Rechargeable nickel–3D zinc batteries: an energy-dense, safer alternative to lithium-ion, Science (2017), https://doi.org/10.1126/science.aak9991.
[13] B. Yan, M.S. Li, X.F. Li, Z.M. Bai, J.W. Yang, D.B. Xiong, D.J. Li, Novel understanding of carbothermal reduction enhancing electronic and ionic conductivity of Li4Ti5O12 anode, J. Mater. Chem. (2015), https://doi.org/10.1039/C5TA00887E.
[14] X. Wang, Q. Weng, Y. Yang, Y. Bando, D. Golberg, Hybrid two-dimensional materials in rechargeable battery applications and their microscopic mechanisms, Chem. Soc. Rev. (2016), https://doi.org/10.1039/C5CS00937E.
[15] Y. Li, Y. Lu, P. Adelhelm, M.M. Titirici, Y.S. Hu, Intercalation chemistry of graphite: alkali metal ions and beyond, Chem. Soc. Rev. (2019), https://doi.org/10.1039/C9CS00162J.
[16] K. Wasalathilake, H. Li, L. Xu, C. Yan, Recent advances in graphene based materials as anode materials in sodium-ion batteries, J. Energy Chem. (2019), https://doi.org/10.1016/j.jechem.2019.06.016.
[17] H.S. Jeong, J. Kim, K. Jo, J. Kee, J.H. Choi, J. Koo, Oriented wrinkle textures of free-standing graphene nanosheets: application as a high-performance lithium-ion battery anode, Carbon Lett. (2021), https://doi.org/10.1007/s42823-020-00163-9.
[18] X. Liu, C.Z. Wang, M. Hupalo, H.Q. Lin, K.M. Ho, M.C. Tringides, Metals on graphene: interactions, growth morphology, and thermal stability, Crystals (2013), https://doi.org/10.3390/cryst3010079.
[19] Z.S. Wu, G. Zhou, L.C. Yin, W. Ren, F. Li, H.M. Cheng, Graphene/metal oxide composite electrode materials for energy storage, Nano Energy (2012), https://doi.org/10.1016/j.nanoen.2011.11.001.
[20] Z. Li, X. Ge, C. Li, S. Dong, R. Tang, C. Wang, Z. Zhang, L. Yin, Rational microstructure design on metal–organic framework composites for better electrochemical performances: design principle, synthetic strategy, and promotion mechanism, Small Methods (2020), https://doi.org/10.1002/smtd.201900756.
[21] D. Nandi, V.B. Mohan, A.K. Bhowmick, D. Bhattacharyya, Metal/metal oxide decorated graphene synthesis and application as supercapacitor: a review, J. Mater. Sci. (2020), https://link.springer.com/article/10.1007%2Fs10853-020-04475-z.

[22] F.J. Soler-Piña, C.H. Rentero, A. Caballero, J. Morales, E.R. Castellón, J.C. Vázquez, Highly graphitized carbon nanosheets with embedded Ni nanocrystals as anode for Li-ion batteries, Nano Res. (2020), https://doi.org/10.1007/s12274-019-2576-4.
[23] R. Siburian, J. Nakamura, Formation process of Pt subnano-clusters on graphene nanosheets, J. Phys. Chem. C (2012), https://doi.org/10.1021/jp307327e.
[24] R. Siburian, T. Kondo, J. Nakamura, Size control to a sub-nanometer scale in platinum catalysts on graphene, J. Phys. Chem. C (2013), https://doi.org/10.1021/jp311852j.
[25] C.M.P. Kumar, T.V. Venkatesha, R. Shabadi, Preparation and corrosion behavior of Ni and Ni–graphene composite coating, Mater. Res. Bull. (2013), https://doi.org/10.1016/j.materresbull.2012.12.064.
[26] D. Zhang, X. Cui, G. Jin, Y. Jiao, D. Li, Preparation, deposited behavior and hydrophobic property of modified graphene oxide reinforced Ni composite coatings by magnetic field assisted electro-brush plating, Surf. Coating. Technol. (2020), https://doi.org/10.1016/j.surfcoat.2020.126363.
[27] A.N. Popova, Crystallographic analysis of graphite by X-Ray diffraction, Coke Chem. (2017), https://doi.org/10.3103/S1068364X17090058.
[28] T. Ohta, A. Bostwick, T. Seyller, K. Horn, E. Rotenberg, Controlling the electronic structure of bilayer graphene, Science (2006), https://doi.org/10.1126/science.1130681.
[29] R. Siburian, Ab M.M. Ali, K. Sebayang, M. Supeno, K. Tarigan, C. Simanjuntak, S. P. Aritonang, F. Hutagalung, The loading effect of Pt clusters on Pt/graphene nano sheets catalysts, Sci. Rep. (2021). https://www.nature.com/articles/s41598-021-80472-1.
[30] T. Abtew, B.C. Shih, S. Banerjee, P. Zhang, Graphene–ferromagnet interfaces: hybridization, magnetization and charge transfer, Nanoscale (2013), https://doi.org/10.1039/C2NR32972G.
[31] S.Y. Lin, N.T.T. Tran, M.F. Lin, Diversified phenomena in metal- and transition-metal-adsorbed graphene nanoribbons, Nanomaterials (2021), https://doi.org/10.3390/nano11030630.
[32] A. Dahal, M. Batzill, Graphene–nickel interfaces: a review, Nanoscale (2014), https://doi.org/10.1039/C3NR05279F.
[33] Y. Dedkov, E. Voloshina, Graphene growth and properties on metal substrates, J. Phys. Condens. Matter (2015), https://doi.org/10.1088/0953-8984/27/30/303002.
[34] S.M. Choi, M.H. Seo, H.J. Kim, W.B. Kim, Synthesis and characterization of graphene-supported metal nanoparticles by impregnation method with heat treatment in H_2 atmosphere, Synth. Met. (2011), https://doi.org/10.1016/j.synthmet.2011.09.008.
[35] F. Montejo-Alvaro, J. Oliva, A. Zarate, M. Herrera-Trejo, H.M. Hdz-García, A. I. Mtz-Enriquez, Icosahedral transition metal clusters (M13, M = Fe, Ni, and Cu) adsorbed on graphene quantum dots, a DFT study, Phys. E Low-dimens. Syst. Nanostruct. (2019), https://doi.org/10.1016/j.physe.2019.02.005.

Developing Nickel/Graphene Nano Sheets as an alternative primary battery anode

ORIGINALITY REPORT

12%	11%	8%	4%
SIMILARITY INDEX	INTERNET SOURCES	PUBLICATIONS	STUDENT PAPERS

PRIMARY SOURCES

1	www.ncbi.nlm.nih.gov Internet Source	3%
2	zaguan.unizar.es Internet Source	2%
3	update.library.uitm.edu.my Internet Source	2%
4	journals.utm.my Internet Source	1%
5	www.researchsquare.com Internet Source	1%
6	profdoc.um.ac.ir Internet Source	1%
7	Kiruthiga Ramakrishnan, Chandrasekaran Nithya, Bindhya Kundoly Purushothaman, Nitesh Kumar, Sukumaran Gopukumar. " Sb O @rGO Nanocomposite Anode for High Performance Sodium-Ion Batteries ", ACS Sustainable Chemistry & Engineering, 2017 Publication	1%

8	repository.usu.ac.id Internet Source	1 %
9	eng.usf.edu Internet Source	1 %

Exclude quotes	Off	Exclude matches	< 1%
Exclude bibliography	On		